DNA as Surrogate for Process Verification in Plasma Inactivation

Abstract:

As an emerging nonthermal processing technology, plasma has drawn lots of attention in food industry in recent years. Plasma technology is highly effective in inactivating various types of food pathogens in solution as well as on food contact surfaces. In addition, plasma technology consumes significant less amount of energy and water resources as compared traditional sanitization. To introduce plasma technology to large scale food industry, the first step would be to establish a process verification methodology. Process verification in plasma technology is difficult as active plasma species are often short lived. Introducing microorganism as surrogate to the processing plant is not desired. Thus, the overall objective of this study is to fill the gap by developing cell free bio-based surrogate to verify plasma based bacterial inactivation. This study developed Chitosan-DNA film as the surrogate for verification of gas plasma as well as plasma activated water. The DNA damage by plasma was characterized with Fourier-transform infrared spectroscopy (FTIR). Through machine learning algorithm, both plasma dosage, inactivation of planktonic cells as well as biofilms could be predicted with high accuracy (>89%) by FTIR spectra. Thus, Chitosan-DNA layer by layer film could be used as a potential surrogate for the verification of plasma efficiency in food industry.

Introduction:

In recent years, there is a rising demand of foods that are healthier, less processed and richer in taste among consumers. This has brought new challenges for food scientist. Microorganism has always been problem causing factor in food industry. Microbes spread across food supply chain causing food spoilage. Pathogens cause foodborne diseases, which have always been a threat to

human health. Sanitizers such as NaOCl, H_2O_2, peracetic acid and ozone are traditional methods to control microorganism in food industry. Recently, nonthermal process, in particular plasma technology, is emerging as novel sanitation method. Plasma is known as neutral ionized gas which is composed of various types of particles including free electrons, radicals, and positive and negative ions. As compared to traditional process, plasma technology does not require expensive operation. It does not introduce potentially harmful disinfectant by-products. More importantly, plasma technology consumes significantly less amounts of water than many traditional processes (Chen, 2018). Plasma technology has shown high efficacy in inactivating different types of microorganisms, from bacteria, fungi, spores to biofilms. For example, atmospheric pressure cold plasma (ACP) generated by argon and 1 mL/L oxygen has achieved a 5 log CFU reduction of *Citrobacter freundii* in apple juice (Surowsky et al). ACP treatment also resulted in 3.57, 6.69 and 6.53 decimal reductions of *Escherichia coli*, *Salmonella typhimurium* and *Listeria monocytogenes* inoculated on agar plates with exposure times of 60 s, 45 s and 7 min respectively (Yong, 2015). Despite promising research findings on plasma technologies, there are some challenges associated with its applications in large scale daily food processing. Food processing is associated with various dynamic processing parameters. The effectiveness of plasma technologies is largely dependent on these processing parameters that are varying across time dimension and space dimension. For example, in fresh produce industry, difference processing batches may contain different amount of organic contents like soil and other debris, which can consume the active plasma radicals and therefore significantly affects the efficacy of plasma treatment (Teng et al., 2018). In addition, the effectiveness of plasma technologies is dependent on various physical characteristics such as the distance of plasma jet to the sample, the jet type, exposure time (Oh et al., 2018).. These conditions are difficult to be consistent in a dynamic batch processing

environment. Therefore, process verification is required to ensure that inactivation of food pathogens is uniformly effective in terms of time and space dimensions.

In food industry, process verification relies on surrogate bacterium whose inactivation profile resembles a target bacterium. A suitable surrogate bacterium for validating plasma efficiency has not been identified (Gombas et al., 2017, Hu et al., 2017). Second, introducing live surrogate bacteria to a processing facility is not a preferred approach for the industry as many sites do not have adequate infrastructure to generate and manage the surrogate bacteria (Coughlan, Cotter, Hill, & Alvarez-Ordóñez, 2016). Unlike thermal processing, sanitation is conducted in an open system which makes it difficult to control surrogate bacteria. Apart from using bacterial surrogate, the mostly likely process validation approaches for plasma treatment at the industry level include the electrical and optical measurements (Cullen, 2017). Such measurements are based on monitoring plasma physics, such as ion species. Such measurements are not directly correlated with bacteria inactivation as bacteria inactivation is complicated by lots of other processing parameters, including treatment time, organic content in the processing facility.

To address above needs, this study proposed using macromolecules, in particular DNA, as surrogate to validate the effectiveness of plasma treatment. Plasma inactivates microbes via cell-lethal reactive species such as reactive oxygen species (ROS) and reactive nitrogen species (RNS) with ROS being the principal contributing species (Cullen, 2015, Joshi, 011). ROS damages cells via triggering oxidative stress, which causes enzyme inactivation and DNA cleavage (Cadet, 2013). It has been proposed that severe damage to intracellular components, in particular DNA has been the leading cause of microbe inactivation in High-Voltage Atmospheric Cold Plasma (HVACP) (Han, 2016). The degree of DNA fragmentation measured by PCR and agarose gel electrophoresis was correlated with inactivation level in *Listeria monocytogenes* (Lu, 2013). Alternatively, DNA

damage can be characterized with vibrational spectroscopy methods (Kuimova, 2006). In this study, DNA damage was characterized with Fourier-transform infrared spectroscopy (FTIR) as it allows for scalability in commercial applications. The main goal is to evaluate whether the DNA based surrogate can be used to predict microbe inactivation. Machine learning algorithm was applied to analyze FTIR data and build predictive model.

Material and method

Bacterial strain and sample preparation

Escherichia coli DH5α was grown overnight (20 h - 24 h) at 37 °C to reach stationary phase in tryptic soy broth (TSB; BDTM, Franklin Lakes, NJ). Cultures were centrifuged, washed, and resuspended in DI water to obtain an initial bacterial concentration of 8-9 log CFU/ml. The washed culture was used for surface inoculation on stainless steel or evaluating the inactivation of PAW in a planktonic system.

Preparation of adherent cells on stainless steel

Strips of multipurpose 304 stainless steel (SS) were purchased from McMaster-Carr® (Elmhurst, IL) and were cut into coupons by 1" × 1". The coupon surfaces were sanitized by dipping into 70 % ethanol for 2 min, rinsed by deionized, and dried in a laminar flow cabinet before use. Overnight grown cultures were centrifuged, washed, and resuspended in DI water. One side of the coupon surface was spot inoculated with 100 µL of bacterial suspension uniformly over the surface. Following inoculation, coupons were dried in a laminar flow cabinet for 1 h at room temperature to allow the adhesion of bacterial cells on the surface.

Preparation of biofilms

Biofilms were grown using the method from Buckingham-Meyer *et al*. with modifications (Buckingham-Meyer, Goeres, & Hamilton, 2007). A layer of sterile filter paper (Whatman Qualitative Grad 2, 100-mm diameter) was placed on top of a tryptic soy agar (TSA) plate. Overnight culture of *E. coli* was diluted 1:10 in TSB and an aliquot of 1.5 mL was transferred onto the filter paper. The air trapped in bubbles between the filter paper and TSA agar were carefully removed with a sterile spreader. Then, 4 pieces of sterile conveyor belt coupons were placed on the top of the inoculated filter paper. The plate was incubated for 24 h at 37 ºC before use.

Evaluation of inactivation efficacy of gas plasma and plasma-activated water (PAW)

Cold atmospheric pressure plasma jet

OPENAIR™ Jet Plasma System (CD50 jet and FG5001 plasma generator) (Plasmatreat Inc., IL, USA) was used in the current study for both the generation of PAW and gas plasma treatment on stainless steel surface. High voltage was maintained between the stator and rotor of the plasma jet motor, which enabled plasma to be discharged through nozzle using working gas. Rotating nozzle was equipped to ensure equal distribution of plasma throughout the exposed surface. The input power of plasma jet was 295 V and the frequency was 22.5 kHz. Compressed air (1190 mBar) was used as working gas in production of plasma.

Preparation of PAW

PAW was produced by exposing deionized water (DI water) to plasma jet described above. The distance between the end of plasma nozzle and the water surface was constant at 5 cm. DI water of 200 mL was filled in a 1 L glass beaker and activated by plasma for 2min, 5 min or 10 min, defined as, PAW2, PAW5, and PAW10, respectively. After plasma activation, A volume of 0.99 mL of PAW was immediately transferred to a 1.5 mL sterile centrifuge tube and rest at room

temperature for 2 min before bacterial treatment to make sure the temperature of PAW was below 35 °C.

Gas plasma treatment on stainless steel surface against adherent E. coli and biofilms

A coupon was placed on top of a rotating platform (~ 80 rpm) with the side of the coupon with adherent cells or biofilms facing the rotating nozzle of the CAPP jet for various treatment times (60 s, 90 s, or 120 s) at a distance of 3 cm. Rotating platform during CAPP treatment was chosen to ensure a uniform distribution of plasma over the coupon surface and to prevent local overheating. Coupon without CAPP treatment was used as control to determine initial the load of bacteria on the surface.

PAW treatment against planktonic E. coli and biofilms

The inactivation efficacy of PAW was evaluated against both planktonic E. coli and biofilms. In a planktonic system, a volume of 0.01 mL of bacterial suspension was added to a centrifuge tube containing 0.99 mL of PAW to reach a concentration of 6-7 log CFU/mL and mixed thoroughly. The mixture was incubated at room temperature (22±2 °C) for 2 min. Following each incubation, the bacterial suspension was serially diluted in DI water and platted on trypticase soy agar (TSA; BDTM, Franklin Lakes, NJ). For biofilm treatment, SS with biofilms developed on the surface was immersed in PAW for 2 min. Then, the bacterial cells were detached and enumerated as described above.

Bacterial recovery and enumeration

Adherent bacterial cells and biofilms were recovered and enumerated using the method of Niemira *et al*. with modifications (Niemira, Boyd, & Sites, 2014). A coupon was placed in a sterile 50 mL centrifuge tube with 10 mL 0.2 % buffered peptone water (BPW) and 10 counts of sterile glass

beads (4 mm in diameter). Then, the centrifuge tube was vortexed vigorously for 1 min to allow detachment of adherent cells or biofilm from the coupon surface. The resuspended cells were then serial diluted in 0.2 % BPW and plated onto TSA. The number of colony-forming units (CFU) was determined by plate counts following incubation of the plates at 37 °C for 24 h. The bacterial reductions in log CFU/mL were determined by subtracting bacterial surviving population of each PAW treatment from the bacterial population of the control.

Evaluation of inactivation efficacy of acidified nitrate and nitrite solutions

Nitrate and nitrite in combination or nitrite only of the same concentrations as PAW2, PAW5 or PAW10 and were prepared in HCl or HNO_3 solution to simulate the nitrogen species identified in PAW. The pH of the acid solution was adjusted to the same value as of PAW2, PAW5, and PAW10, respectively. Stationary phase *E. coli* culture was diluted, incubated in the acidified nitrite or mixture solution, and enumerated after the treatment as described above.

Characterization of the physicochemical properties of PAW

Oxidation-reduction potential (ORP), electrical conductivity (EC), and pH

ORP, EC, and pH were measured using an Orion Star™ A325 portable pH/Conductivity meter with an 8107UWMMD Orion ROSS Triode pH/ATC gel-filled electrode (ThermoFisher, Waltham, MA). The probe was immersed in the solutions until a stable reading is obtained. Each measurement was performed immediately after plasma activation of DI of a selected duration.

Determination of nitrate and nitrite concentration from PAW

Nitrate and nitrite concentrations in PAW as a function of plasma activation duration was measured based on the method by Miranda *et al*. (Miranda, Espey, & Wink, 2001). Stock solutions

of vanadium (III) chloride (VCl_3) (400 mg) were prepared in 1 M HCl (50 mL) and stored in dark at 4 °C. N-(1-Naphthyl)ethylenediamine dihydrochloride (NEDD) of 0.1% w/v in DI and sulfanilamide (SULF) of 2% w/v in 5% HCl were prepared with stirring and heating, after which each solution was filtered to remove trace particulates and stored in dark at 4 °C. To detect the concentration of total NOx (nitrate and nitrite), PAW samples of various plasma activation duration were transferred (100 μL) to a 96-well, clear plate, following by loading 100 μL of VCl3 to each well and rapidly following by addition of SULF (50 μL) and NEDD (50 μL). The absorbance at 540 nm was measured using a plate reader following incubation for 30 min at room temperature. Nitrite concentration was measured in a similar manner except that no VCl3 was added to the wells. Nitrate concentration was determined by subtracting nitrite from the total NOx concentration. Linear regression of the mean values of the absorbance at 540 nm for each of a NOx and nitrite standard was utilized to determine the nitrate/nitrite concentrations.

Substrate preparation

Chitosan-DNA substrate was prepared by coating Chitosan-DNA film on stainless steel coupon. 10 mg/ml Salmon sperm DNA 40 ul was added to stainless steel and dried in room temperature. Then, another layer of chitosan dissolved in sodium acetate/acetic acid pH 4.76 was spread on top of DNA layer and dried at room temperature.

FTIR measurement

The recovered DNA after NaOCl treatment was spotted on anodisc membranes (0.2 mm pore size, 13 mm OD) and dried with filtration system. DNA formed a relatively uniform thin layer upon deposition. It has been shown that the anodisc membrane filter does not contribute spectral features between 400 and 4000 cm^{-1}.

Random spots on anodisc membranes were chosen for spectra collection. FTIR spectra were collected using IRPrestige-21 FTIR spectrometer (Shimadzu Co., Kyoto, Japan). The anodisc filter containing a uniform thin layer of DNA was placed directly on the diamond crystal cell of attenuated total reflectance (ATR). Spectra was collected from 4000 to 400 cm-1 at a resolution of 2 cm-1 by adding together 32 interferograms.

FTIR data processing and data modelling

FTIR data was analyzed with Python by running Jupiter Notebook. Raw FTIR data in text format was loaded into Jupyter Notebook and converted to Pandas DataFrame with Python Pandas library. Principal component analysis PCA was first conducted with scikit-learn library PCA package.

Then, LightGBM model was implemented with scikit-learn library. To investigate the model performance to unseen data set, 5-fold Cross validation was conducted by splitting the data set to 5 folds and making prediction with one-fold using other 4 folds. Predictions was evaluated with following metrics and prediction errors was averaged among the 5 folds. Receiver Operating Characteristic (ROC) curve and Confusion Matrix (CM) were used as metrics to assess LightGBM model performance. Feature importance plot was also obtained with Python.

Statistical analysis

Throughout the study, experiments were conducted in three independent trials. Measurements will be conducted in three replicates and reported values were in the form of averaged values ± standard deviation. Analysis of Variance (ANOVA) will be used to determine statistical significance and $p<0.05$ is considered as significance.

Result and Discussion

Inactivation efficacy of PAW on planktonic *E. coli* and biofilms

Figure 1 represents the reduction in microbial load of planktonic *E. coli* and its biofilms by PAW2, PAW5, and PAW10. In a planktonic system (**Figure 1 A**), *E. coli* was reduced by 1.1±0.3 log CFU/mL incubated in PAW2 for 2 min. PAW5 and PAW10 achieved a significantly higher ($p<0.05$) numbers of reduction of population than PAW2 (>5 log CFU/mL of *E. coli* was inactivated). Bacteria incubated in DI water did not show any significant reduced numbers of population. When PAW was applied on inactivation of *E. coli* biofilms (**Figure 1 B**), the inactivation efficacy of PAW2 (2.2±0.2 log CFU/inch^2), PAW5 (3.6±0.8 log CFU/inch^2), and PAW10 (4.4±0.5 log CFU/inch^2) was significantly ($p<0.05$) different from each other, with PAW of a higher plasma activation duration demonstrated a higher microbial inactivation efficacy. These observations are consistent with previous reports that the duration of water being exposure to plasma have impacts on the inactivation efficacy of PAW (Kamgang-Youbi et al., 2009; Xiang et al., 2018; Zhang et al., 2016). In addition, PAW was more effective against planktonic cells than biofilms, as PAW5 reduced >5 log CFU/mL of *E. coli* in a planktonic system whereas 3.6±0.8 log CFU/inch^2 of cells of 24 h biofilms were inactivated by the same PAW. Kamgang *et al*. also reported similar observation that biofilm cells of *Staphylococcus epidermidis* was more resistant towards the treatment by gliding discharge in humid air (Kamgang, Briandet, Herry, Brisset, & Naïtali, 2007). It is likely that the extracellular polysaccharide matrices within biofilms block the penetration of antimicrobial species in PAW resulting in a higher resistance of biofilm cells (Fraise, Maillard, & Sattar, 2012).

A

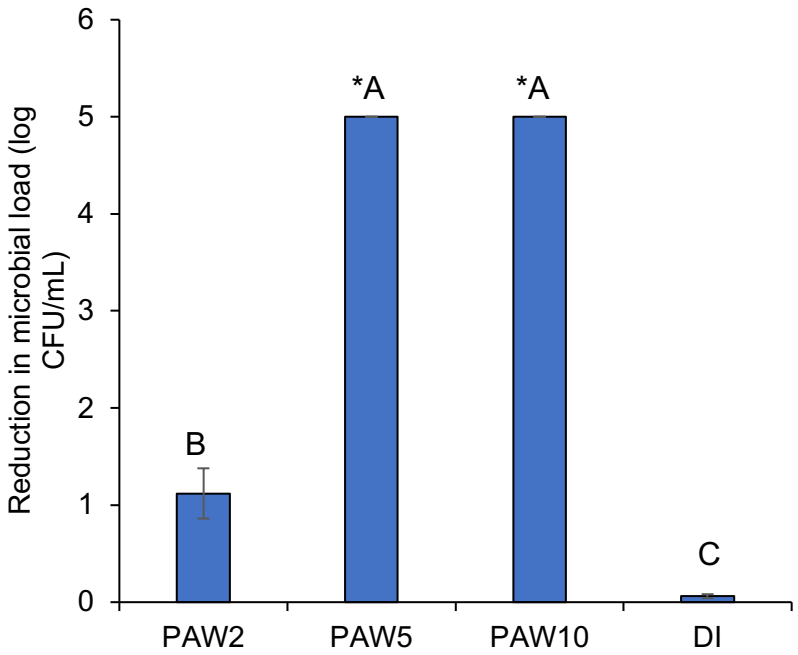
Reduction in microbial load (log CFU/mL)
6
5
4
3
2
1
0
B
*A
*A
C
PAW2
PAW5
PAW10
DI

B

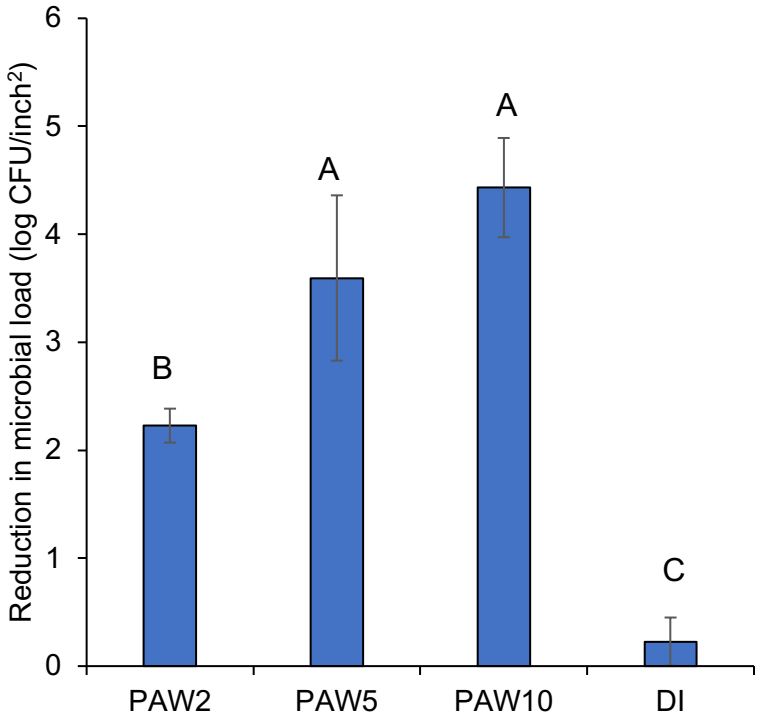
Reduction in microbial load (log CFU/inch²)
6
5
4
3
2
1
0
B
A
A
C
PAW2
PAW5
PAW10
DI

Figure 1 (A) Inactivation efficacy of PAW2, PAW5, and PAW10 on planktonic *E. coli*. (B) Inactivation efficacy of PAW2, PAW5, and PAW10 on 24 h biofilms of *E. coli*.

Inactivation efficacy of gas plasma on adherent *E. coli* and biofilms on stainless steel

Inactivation of adherent cells and biofilms of *E. coli* by CAPP for 60 s, 90 s, or 120 s and at a fixed distance of 3 cm is presented in **Figure 2**. As the **Figure 2A** depicts, gas plasma treatment of 60 s inactivated 3.9±0.6 log CFU/inch^2 of adherent cells, while a treatment time of 90 s or 120s inactivated >4.6 log CFU/inch^2 of adherent cells. As for inactivation against *E. coli* biofilms (**Figure 2B**), a treatment time of 60 s and 90 s achieved the numbers of rection of 2.2±0.8 log CFU/inch^2 and 2.8±0.7 log CFU/inch^2, respectively. A significant increase ($p<0.05$) in inactivation efficacy from 90 s to 120 s (>4.6 log CFU/inch^2) of gas plasma treatment on biofilms was also observed. Similar to what we have observed in the treatment by PAW, gas plasma inactivated a lower number of biofilms cell than adherent cells on stainless steel given a treatment time of 60 s or 90 s , indicating biofilms behaved more resistant towards the reactive species in the gas plasma than adherent cells. In general, a higher level of inactivation can be achieved with an increase in gas plasma treatment time for both adherent cells and biofilms.

A

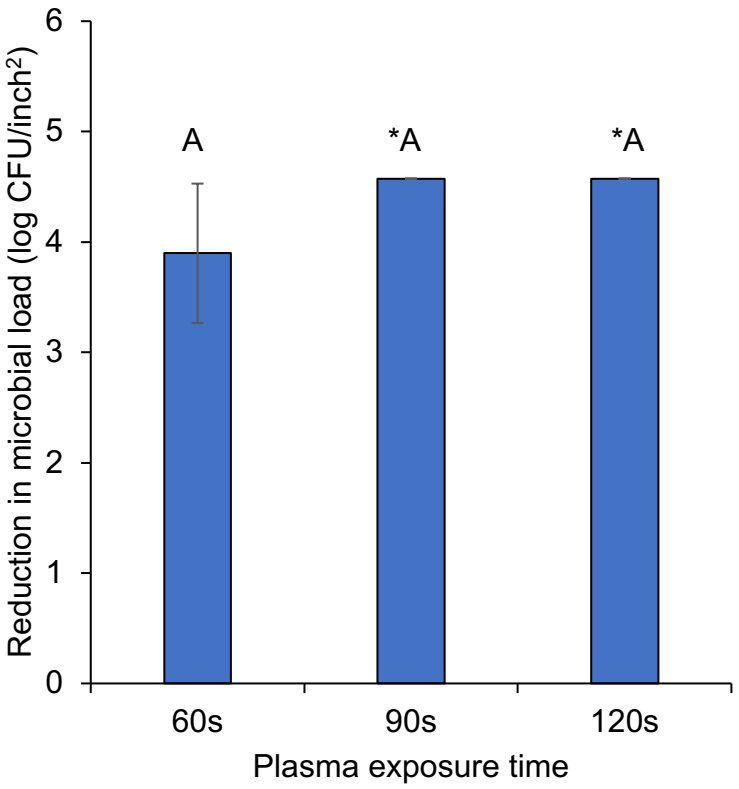
Reduction in microbial load (log CFU/inch²)
6
5
4
3
2
1
0
A
*A
*A
60s
90s
120s
Plasma exposure time

B

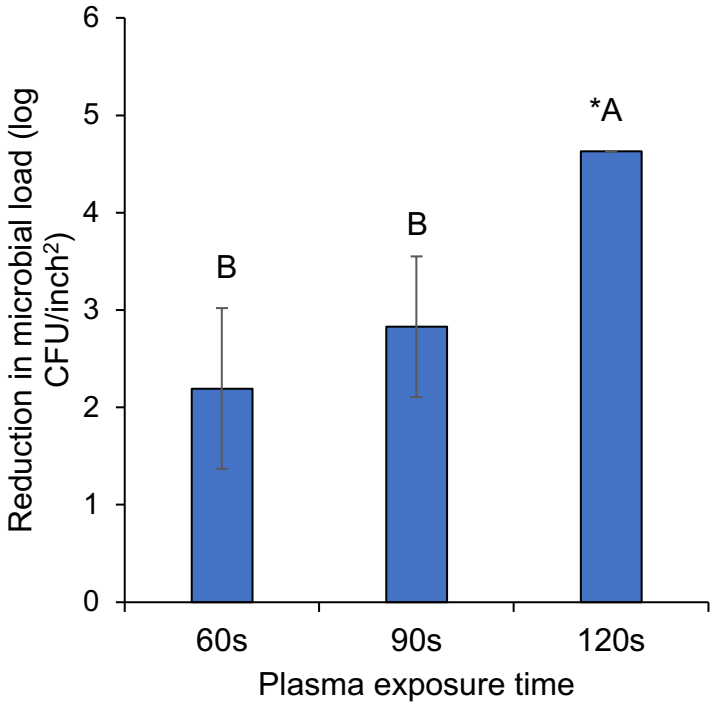
Reduction in microbial load (log CFU/inch²)
6
5
4
3
2
1
0
B
B
*A
60s
90s
120s
Plasma exposure time

Figure 2 Inactivation efficacy of gas plasma on (A) adherent *E. coli* cells and (B) 24 h biofilms of *E. coli* on the surface of stainless-steel coupons as a function of plasma exposure time. All experiments were in triplicate. Mean ± SD.

Inactivation efficacy of acidified NOx solutions

To evaluate the potential antimicrobial efficacy of nitrogen species in PAW, nitrate and nitrite mixtures (NOx) were prepared in HCl to simulate the same concentrations of species and pH values as of PAW2, PAW5, and PAW10, respectively. The inactivation efficacy of the acidified NOx solutions was shown in **Figure 3.2.3**. Interestingly, NOx-5 (NOx concentration corresponding to PAW5) showed a significantly higher ($p<0.05$) inactivation efficacy than that of NOx-10, followed by NOx-2. Since PAW5 contained the highest amount of nitrite than PAW10 and PAW2, nitrite rather than nitrate was more likely to be the species that lead to the inactivation of bacteria in this acidified NOx system. However, this was not consistent with what was observed in PAW where PAW of the longest plasma activation duration (PAW10) demonstrated the highest inactivation efficacy. In addition, PAW was able to render a higher level of inactivation than their corresponding acidified NOx solutions. For example, PAW5 showed a significantly ($p<0.05$) higher numbers of reduction (>5 log CFU/mL) than NOx-5 (1.7±0.4 log CFU/mL in 2 min. Therefore, although nitrite being an effective antimicrobial in an acidified environment, other ingredients in PAW other than nitrate and nitrite were likely to play a role in the inactivation process by PAW.

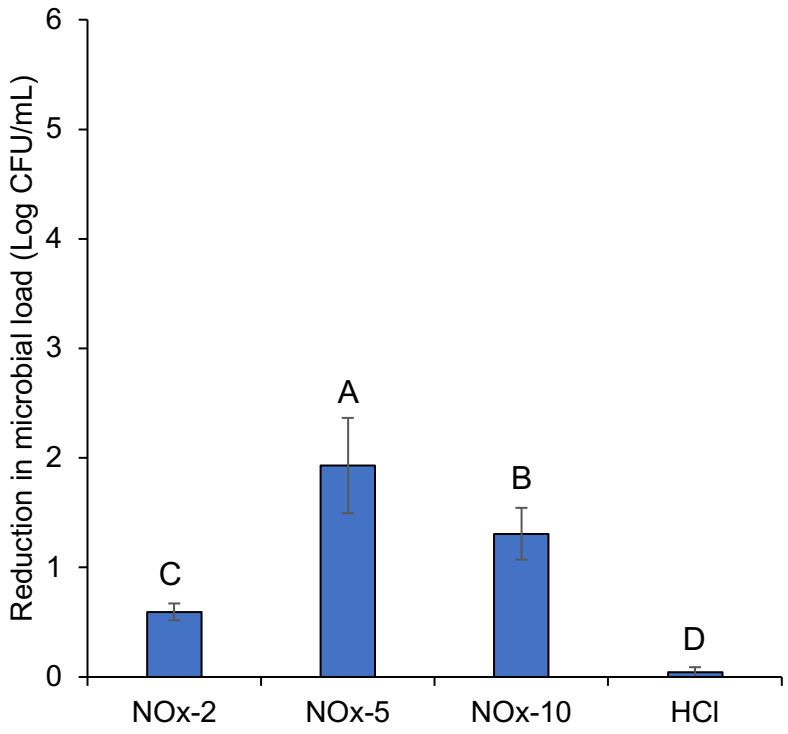

Figure 3 Inactivation efficacy of acidified NO_3 and NO_2 mixture in HCl. The pH value and the concentrations of N_{O3} and NO_2 were the same as of PAW2, PAW5, and PAW10, respectively. HCl without NO_3 or NO_2 was used as control. All experiments were in triplicate. Mean ± SD.

Characterization of PAW

The physicochemical parameters including oxidation-reduction potential (ORP), electrical conductivity (EC), pH value, and the concentrations of nitrite and nitrate of PAW were characterized as a function of plasma activation duration (**Figure 4**). The pH value has been shown to play an important role for the microbial inactivation efficacy, since the structure and function of the biological macromolecules might be affected by high level of H+. As depicted in **Figure 4A**, the pH value of DI water dropped from 6.57±0.12 to 3.18±0.04 after exposure to plasma for 1 min and continuously lowered to 2.58±0.16 and 2.11±0.03 after 10 and 15 min, respectively, showing plasma treatment lead to the acidification of water. This acidification was mainly due to

the formation of nitric acid and was an indicator of the antimicrobial activity of PAW, as lower pH is more favorable for the reactive species to remain stable and to penetrate bacterial membrane (R. Ma et al., 2016). ORP is an important factor affecting the microbial inactivation as a high ORP can damage bacterial membrane and inactivate the defense mechanism of the cells (Liao, Chen, & Xiao, 2007). As shown in **Figure 4**, the ORP value markedly increased from 86.5 to 204.7±2.3 mV after plasma activation for 1 min and reached 239.7±3.0 after 10 min. This increased ORP indicated a significant amount of reactive species were generated in PAW, which have been considered to play an important role in antimicrobial activity of PAW. A linear increase of EC over the plasma treatment time was observed (**Figure 4** C). The EC value of DI water increased from 5.0 μS/cm to 244.6±20.1 μS/cm after 1 min of activation by plasma and increased up to 709.4±31.5 μS/cm after 10 min, indicating the generation of active ions. To identify possible antimicrobial reactive species within PAW, chemical analysis of PAW for the existence of nitrate and nitrite was performed. **Figure 4** D showed that there was a significant increase of nitrate concentration (2.9±0.2 mM, 4.5±0.5 mM, and 5.0±0.2 mM after 2 min, 5 min, and 10 min) during plasma treatment. Different from nitrate, the concentration of nitrite started to decrease after reaching maximum value of 2.6±0.2 μM at 5 min (**Figure 4** E). This observation indicates that nitrite is likely to be converted into other NO species. Similar observations have been reported by Ma *et al.* and Zhou *et al*., and they attributed the decay of nitrite in PAW to the conversion of nitrite to unstable nitrite acid and then decompose into other nitrogen species such as nitric oxide, nitrate, and peroxynitrite (M. Ma, Zhang, Lv, & Sun, 2020; Zhou et al., 2018).

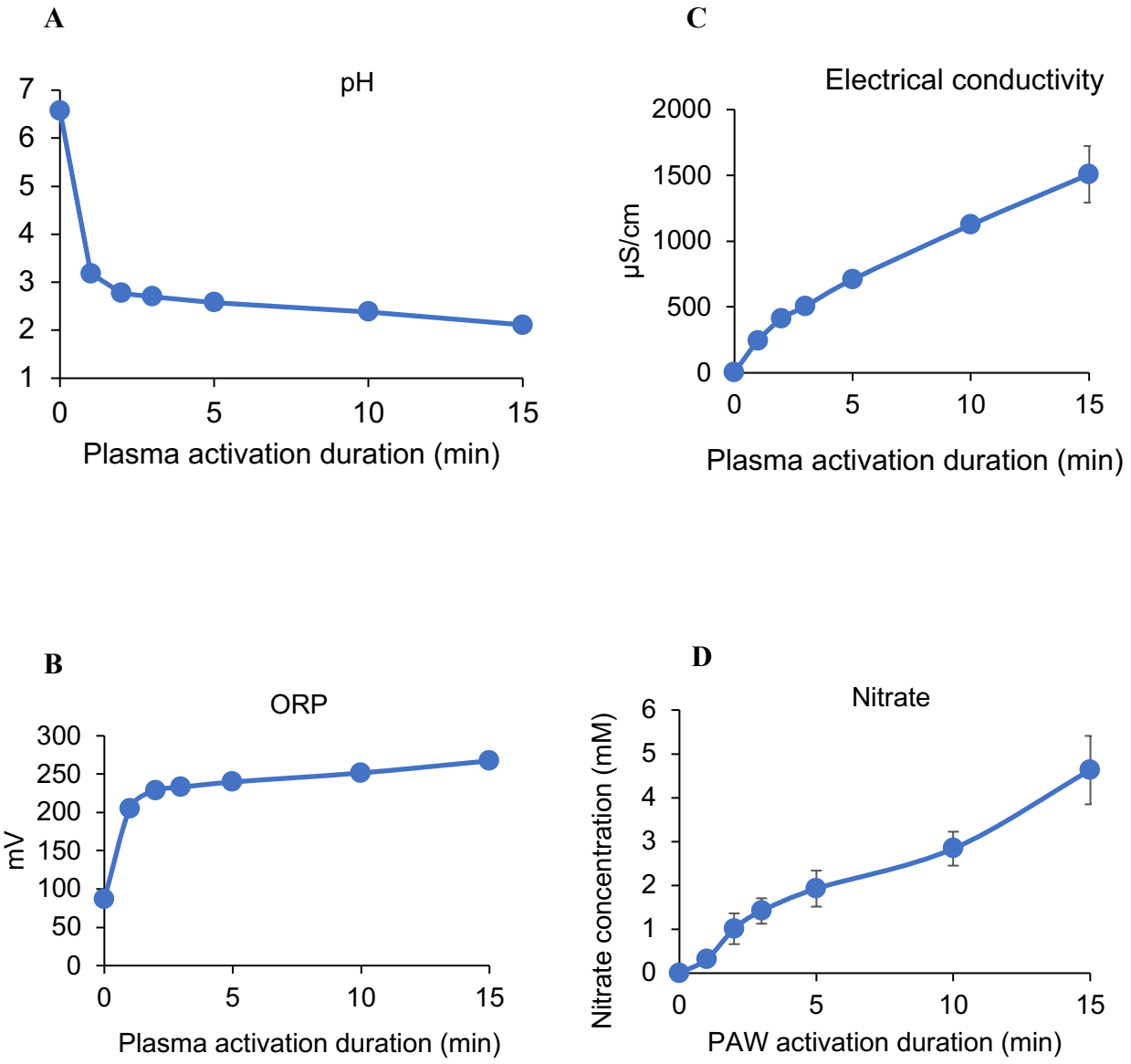
A
pH
7
6
5
4
3
2
1
0
5
10
15
Plasma activation duration (min)
C
Electrical conductivity
2000
1500
1000
500
0
µS/cm
0
5
10
15
Plasma activation duration (min)
B
ORP
300
250
200
150
100
50
0
mV
0
5
10
15
Plasma activation duration (min)
D
Nitrate
6
5
4
3
2
1
0
Nitrate concentration (mM)
0
5
10
15
PAW activation duration (min)

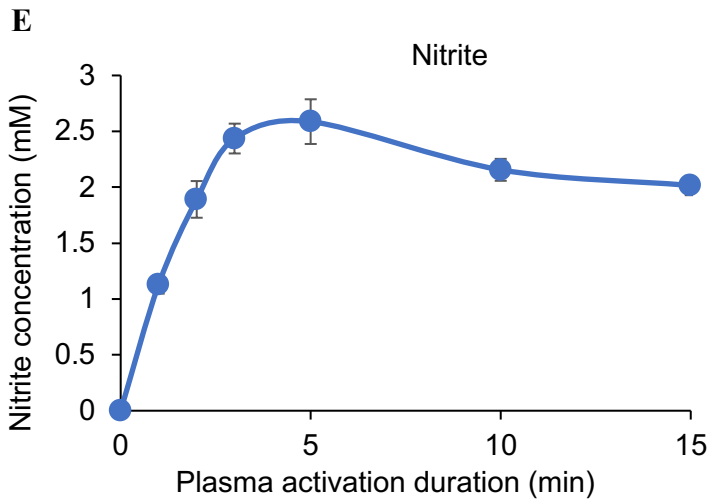

Figure 4 Characterization of PAW of various plasma activation duration. (A) pH (B) Oxidation-reduction potential (ORP). (C) Electrical conductivity. (D). Concentration of nitrate. (E) Concentration of nitrite. All experiments were in triplicate. Mean ± SD.

Prediction for PAW treatment

Plasma-activated water (PAW), an emerging replacement for chlorine solution, can be produced via major two approaches: via contact of plasma stream with water surface or via direct introduction of plasma particle into the water (Thirumdas et al., 2018). The PAW in this study was generated via the first approach. Prediction of the efficacy of plasma treatment involved three aspects: treatment dosage prediction, prediction for bacteria inactivation and biofilm inactivation. Hyperparameters and their values in the LightGBM model were as follows: learning rate 0.0005, bagging fraction 0.7083, bagging frequency 1, lambda l1 0.2634, loss function multi-log loss throughout this study.

Dosage

Figure 5 showed the ROC and confusion matrix for predicting level of PAW treatment, including 0 min (class 0), 2 min (class 1), 5 mins (class 2) and 10 mins (class 3). A ROC curve is a plot of sensitivity on the y axis against (1−specificity) on the x axis for varying values of the threshold t (Zou, O'Malley, & Mauri, 2007). Sensitivity is defined as number of true positive samples (TP) / number of true positive or false negative (FP) samples. Specificity is defined as number of true negative samples / number of true negative or false positive samples. Threshold is the cut off probability for defining positive class. The 45° diagonal line connecting (0,0) to (1,1) in the ROC curve corresponds to random chance. The area under the ROC curve (AUC) is a summary measure that essentially averages diagnostic accuracy across the spectrum of test values. ROC is a suitable metric for balanced classification problem (Kotsiantis, Kanellopoulos, & Pintelas, 2006). Confusion matrix on the other hand provides a straightforward view of the number of data samples that have been correctly or incorrectly classified. In this result, for all 4 levels of plasma treatment, ROC curves oriented towards the top left corner, indicating good prediction accuracy. AUC for ROC curves among all 4 plasma treatment levels reached >0.95, indicating good model performance. AUC result was consistent with the Confusion Matrix. In the confusion matrix, classified samples are located in the diagonal part of the matrix. The total percentage of true classification was 85% among a total of 114 samples. The mechanism for predicting plasma dosage level was likely due to the relationship between dosage level and generated species, which impacted the FTIR spectrum of Chitosan-DNA. Oh *et al.* reported that plasma jet exposure time principally affected the total reactive oxygen and nitrogen species (Oh et al., 2018). Current available diagnostic tools for PAW characterization include ion chromatography, peroxotitanyl spectrometry and classic acid-base titration (Hoeben et al., 2019). As compared to these methods, current study proposed a simple reference tool suitable for PAW synthesis process feedback

control and also for PAW activity monitoring on locations, where only limited laboratory facilities are available.

A

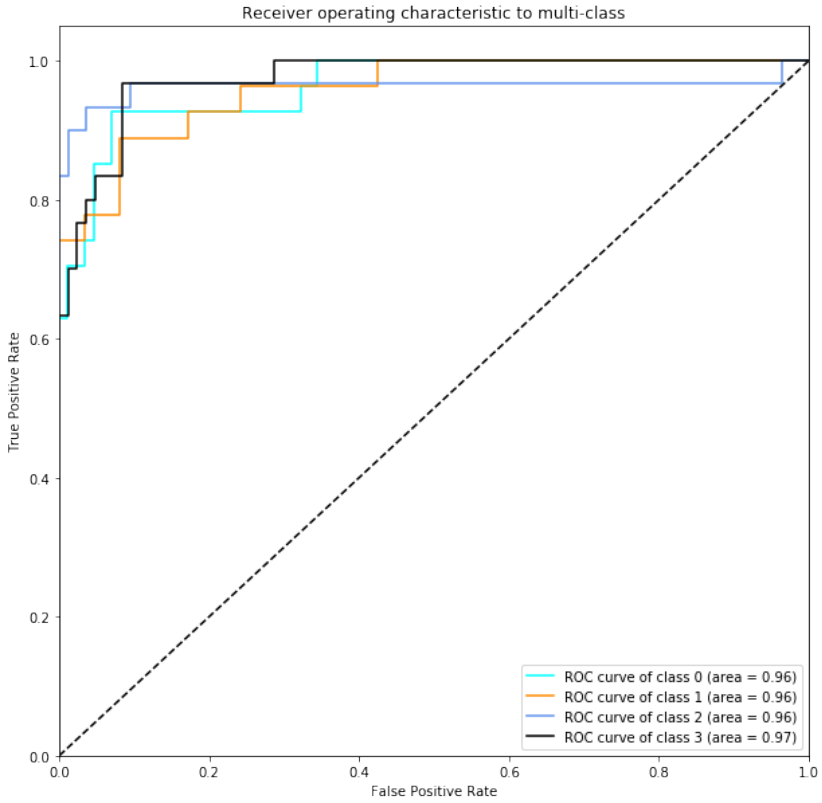

B

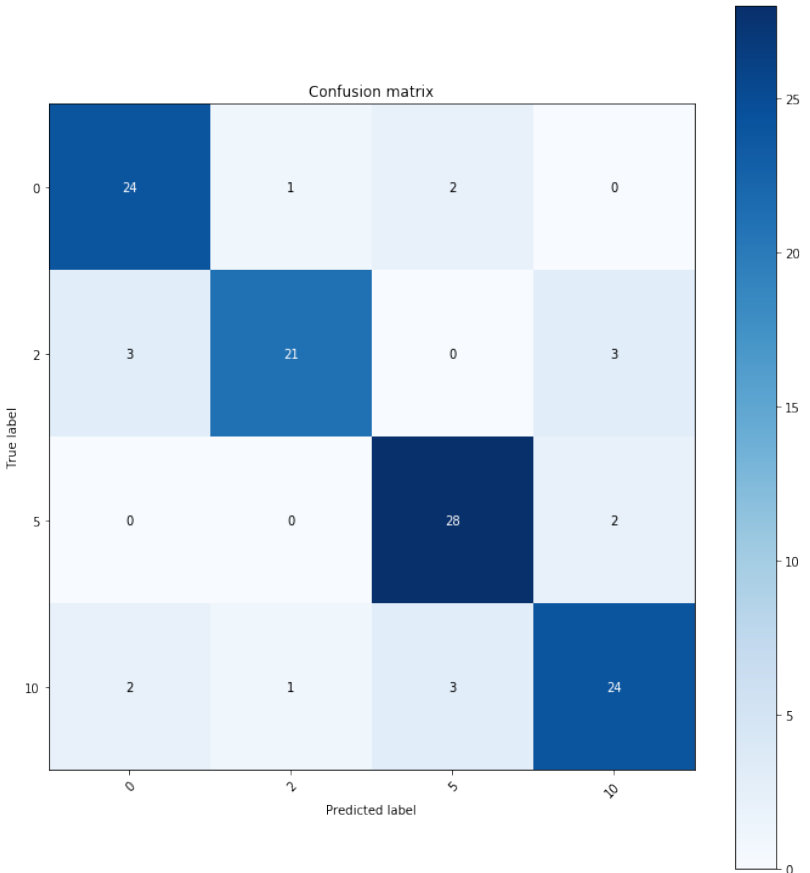

Figure 3.2.5 (A) Receiver operating characteristic plot (B) Confusion matrix for prediction of PAW dosage

Inactivation of planktonic E. coli

Figure 6 showed the prediction of *E. coli* planktonic bacteria inactivation with FTIR data collected from Chitosan-DNA based surrogate. *E. coli* inactivation was grouped into 3 classes, namely 0 log reduction (class 0), 1 log reduction (class 1), 5 log reduction (class 2). ROC curves showed well prediction performances for class 0 and class 1. AUC for class 0 and class 1 were optimal, respectively 0.94 and 0.95. AUC for class 2 were suboptimal at the value of 0.83. This indicated that predicting bacterial inactivation was more challenging than predicting plasma dosage, which was likely due to the more complex relationship between DNA damage with bacteria inactivation as compared to plasma treatment condition. The confusion matrix also showed good prediction performance of the model. The total percentage of true classification was 89% among a total of 114 samples. The efficiency of PAW to kill pathogens is affected by various factors such as the distance of plasma jet to the water, the jet type in addition to the plasma jet exposure time (Oh et al., 2018). Thus, the ability of directly monitoring potential bacterial inactivation level using Chitosan-DNA is critical. Lin *et al.* have been optimizing the biocidal effect of PAW by comparing bacterial counts for all combinations of processing parameters including jet power, water source and activation time (C. M. Lin et al., 2019). With Chitosan-DNA, searching for the optimal treatment condition can be completed in shorter amount of time.

A

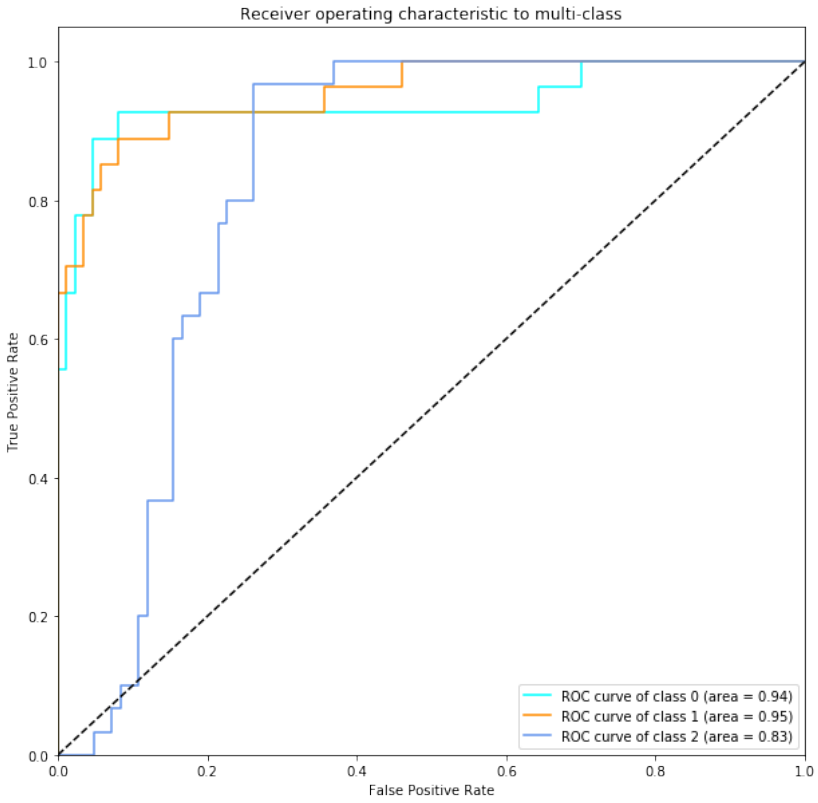
Receiver operating characteristic to multi-class
True Positive Rate
False Positive Rate
0.0
0.2
0.4
0.6
0.8
1.0
ROC curve of class 0 (area = 0.94)
ROC curve of class 1 (area = 0.95)
ROC curve of class 2 (area = 0.83)

B

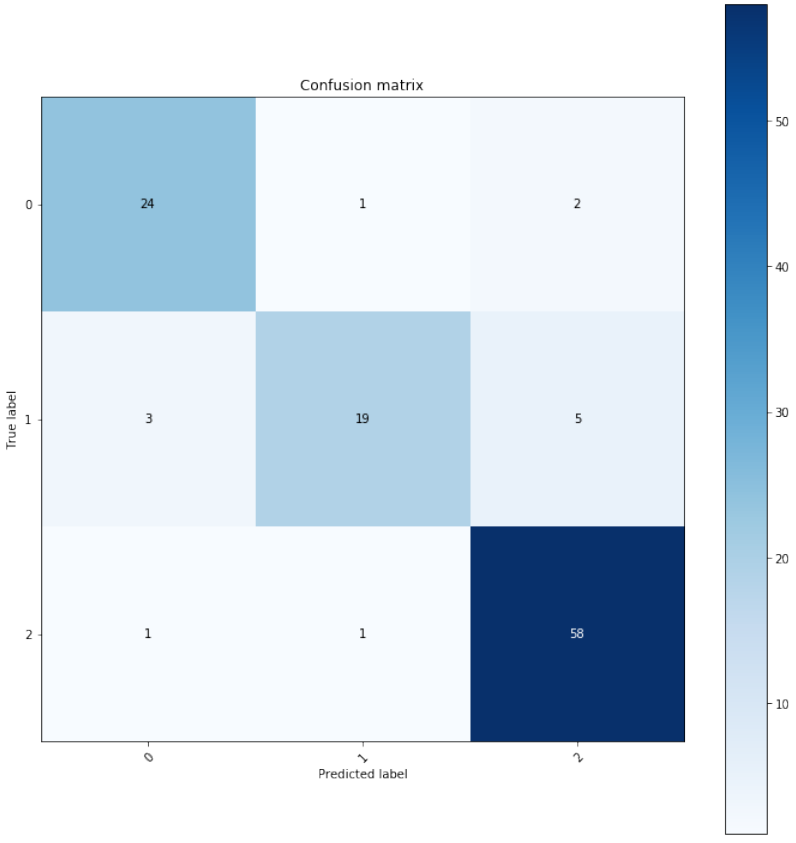
Confusion matrix
True label
Predicted label
24
1
2
3
19
5
1
1
58
0
1
2
50
40
30
20
10

Figure 6 (A) Receiver operating characteristic plot (B) Confusion matrix for prediction of *E. coli* inactivation by PAW

Biofilm Inactivation

Figure 7 showed the prediction of inactivation of *E coli* biofilm with FTIR data of DNA based surrogate. Similar to inactivation of planktonic bacteria, biofilm inactivation fell into 3 classes. ROC curve showed very good model prediction performance for all classes. The confusion matrix also showed good prediction performance of the model. The total percentage of true classification was 89% among a total of 114 samples. Few studies have been related to predicting biofilm inactivation potential by PAW. Smet *et al.* fitted a survival kinetics model for biofilm inactivation and compared the coefficients between biofilm and planktonic cells (Smet et al., 2019). Such model could not be used for process verification.

A

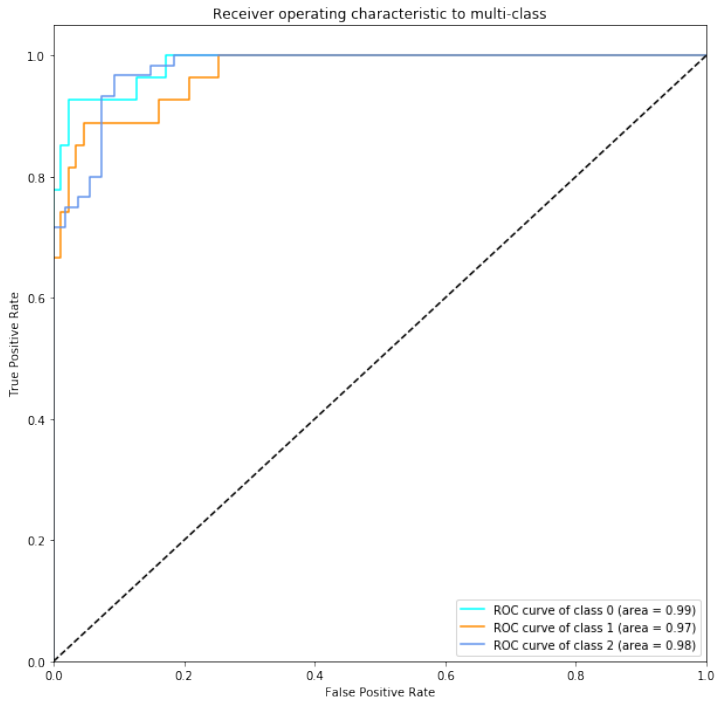

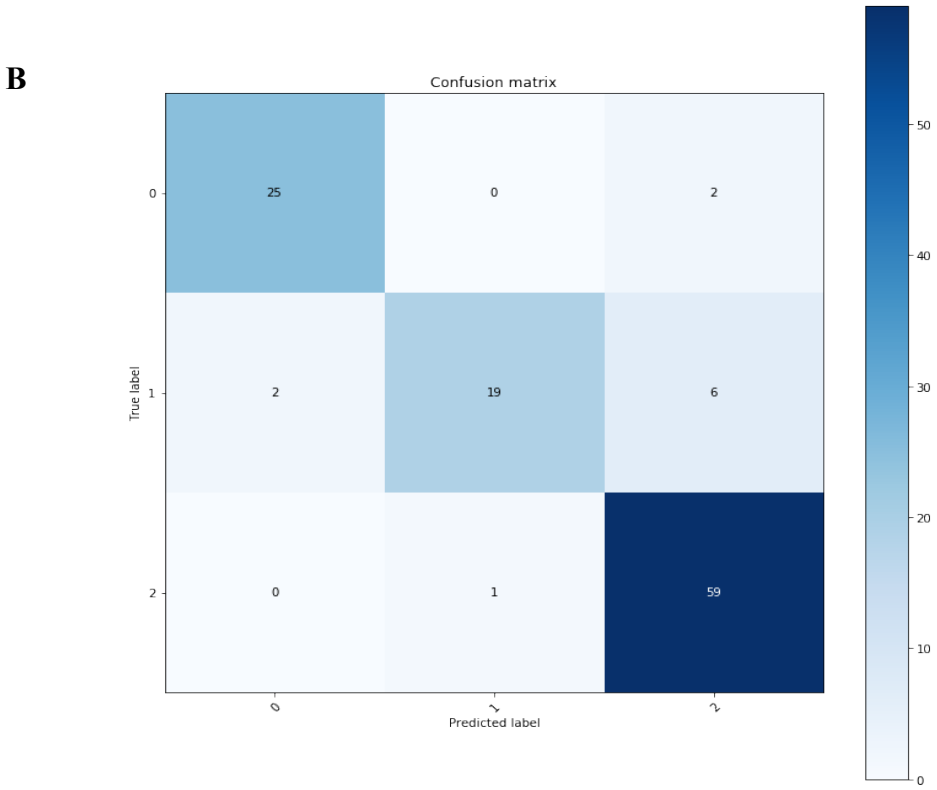

Figure 7 (A) Receiver operating characteristic plot (B) Confusion matrix for prediction of *E. coli* biofilm inactivation by PAW

Prediction for gas plasma treatment

As compared to PAW, gas plasma treatment is a more powerful oxidizing reagent as part of highly effective species generated by plasma such as reactive species have short lifespan (Guo et al., 2018). On the other hand, for gas plasma, it is also more difficult to control the dosage (Thirumdas et al., 2018). Process verification for gas plasma-based sanitation is therefore even more important.

Dosage

Figure 8 showed the prediction of gas plasma treatment level with FTIR data collected from DNA based surrogate. ROC curve showed the model prediction performances are good for all classes with AUC for all classes being above 0.99. The confusion matrix also showed good prediction performance of the model. The total percentage of correct classification was 93% among a total of 114 samples. Bernard *et al.* used lysozyme as a protein model to assess the effect of gas plasma exposure time on protein inactivation as the approach to validate plasma efficacy. The enzyme inactivation was has tested by enzyme-linked immunosorbent assay (ELISA) and a surface plasmon resonance (SPR)-based biosensor assay (Bernard et al., 2006). In comparison, the present study utilized inexpensive sensing molecules and built predictive model that allowed precise monitoring of effective gas plasma applied on samples for scale-up applications. In addition to the application in fresh produce industry, cold atmospheric plasma has emerging applications in biomedical industry. Gas plasma has shown tremendous potential in elimination of cancer cells *in vitro* and *in vivo* (Binenbaum et al., 2017). On the other hand, its efficacy is influenced by physiochemical parameters. In addition to gas plasma exposure time, other parameters that affect the gas plasma efficiency include gas plasma voltage and gas flow rate. The present study inspired the rapid feedback monitoring and validation for these parameters as well.

A

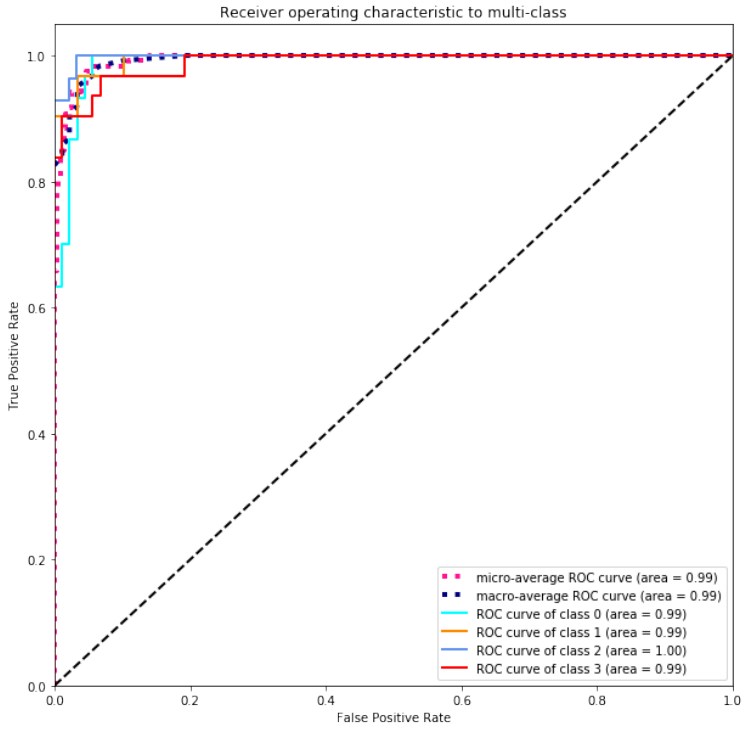
Receiver operating characteristic to multi-class
True Positive Rate
False Positive Rate
0.0
0.2
0.4
0.6
0.8
1.0
micro-average ROC curve (area = 0.99)
macro-average ROC curve (area = 0.99)
ROC curve of class 0 (area = 0.99)
ROC curve of class 1 (area = 0.99)
ROC curve of class 2 (area = 1.00)
ROC curve of class 3 (area = 0.99)

B

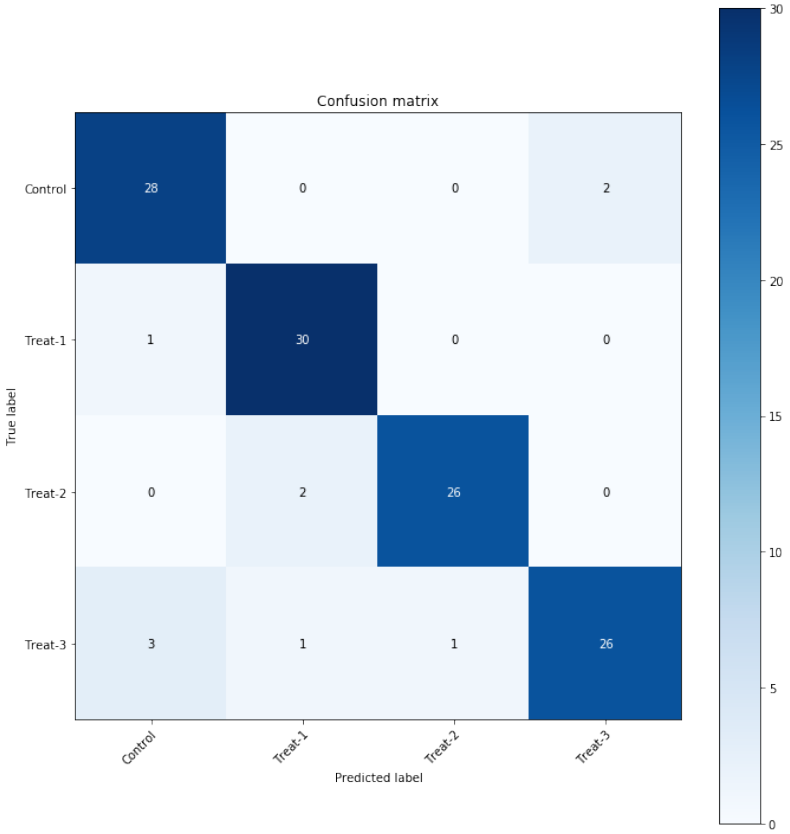
Confusion matrix
Control
Treat-1
Treat-2
Treat-3
True label
Predicted label
28
0
0
2
1
30
0
0
0
2
26
0
3
1
1
26
0
5
10
15
20
25
30

Figure 8 (A) Receiver operating characteristic plot (B) Confusion matrix for prediction of gas plasma dosage

Bacterial Inactivation

Similar to PAW, the biocidal efficacy gas plasma is dependent on various parameters, such as gas composition, the amount of free water in the system (Dobrynin, Fridman, Friedman, & Fridman, 2009). Thus, the ability of predicting bactericidal effect from Chitosan-DNA is critical. **Figure 9** showed the prediction of *E. coli* planktonic bacteria inactivation with FTIR data collected from DNA based surrogate. *E. coli* inactivation was grouped into 3 classes, namely 0 log reduction (class 0), 4 log reduction (class 1), >=5 log reduction (class 2). Similar to dosage prediction, AUC for all classes were close to 0.98. According to confusion matrix, the total percentage of true classification was 96% among a total of 114 samples. Despite that significant amounts of studies have focused on proving the effectiveness of gas plasma in inactivating foodborne pathogens, few studies have aimed at building a process verification system for bacterial inactivation under gas plasma treatment (Shintani, Sakudo, Burke, & McDonnell, 2010).

A

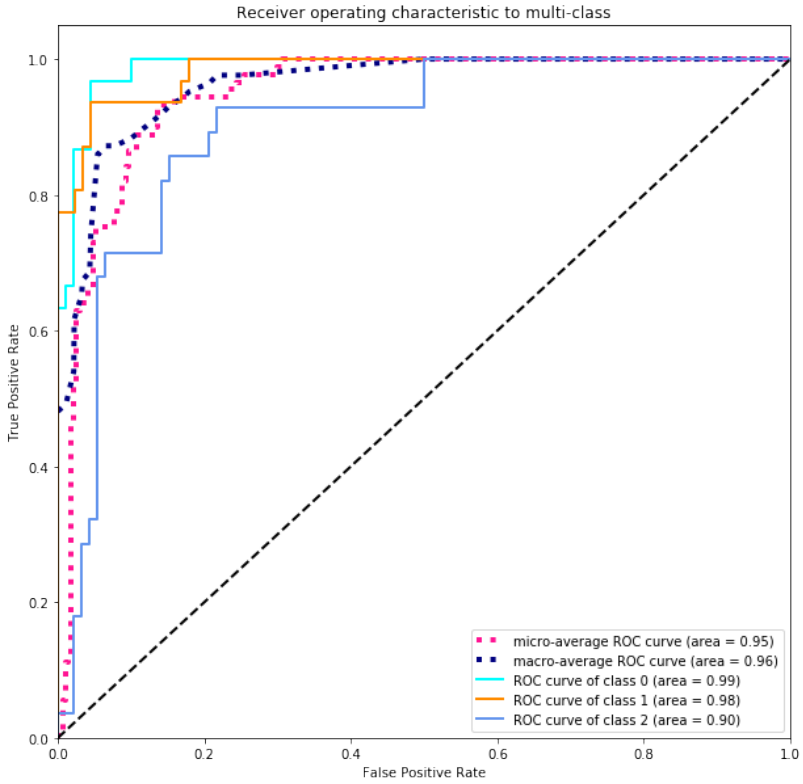
Receiver operating characteristic to multi-class
True Positive Rate
False Positive Rate
0.0
0.2
0.4
0.6
0.8
1.0
micro-average ROC curve (area = 0.95)
macro-average ROC curve (area = 0.96)
ROC curve of class 0 (area = 0.99)
ROC curve of class 1 (area = 0.98)
ROC curve of class 2 (area = 0.90)

B

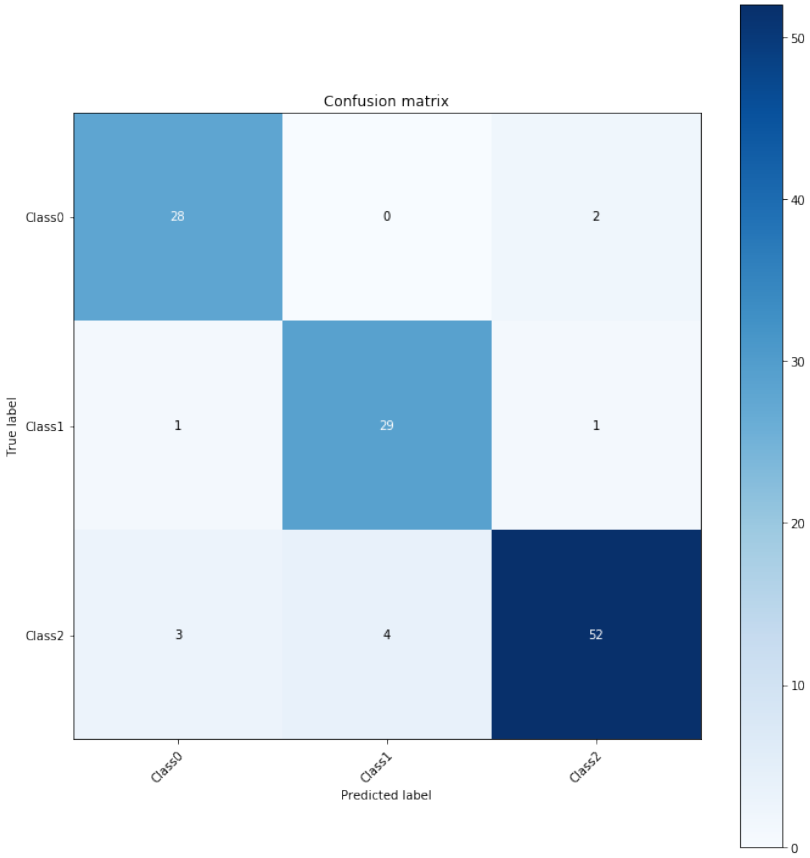
Confusion matrix
Class0
Class1
Class2
True label
Predicted label
28
0
2
1
29
1
3
4
52
0
10
20
30
40
50

Figure 9 (A) Receiver operating characteristic plot (B) Confusion matrix for prediction of *E. coli* inactivation by gas plasma

Biofilm Inactivation

In the case of gas plasma triggered biofilm bacteria, four classes of inactivation were observed, respectively 0 log (class 0), 2 log (class 1), 3 log (class 2) and 5 log (class 3) reduction. Prediction of biofilm inactivation levels was perfect with AUC for all classes being above 0.99 (**Figure 10**). Also, from confusion matrix, the total percentage of true classification was 91% among a total of 114 samples. The prediction for biofilm inactivation was slightly better than the prediction for bacterial inactivation. When predicting bacterial inactivation, data from 90s group and 120s group were merged into the same group, which increased the entropy in the dataset and potentially decreased prediction accuracy. The majority of environmental biofilms contain multiple species. These species can establish cooperative and competitive interactions which may result in an increase resistance to plasma treatment (Govaert, Smet, Walsh, & Van Impe, 2019). The methodology proposed in this study i.e. spectroscopy measurement on Catalase-DNA surrogate plus Machine Learning algorithm for data analysis can be easily adapted to model multi-species biofilm inactivation in the future.

A

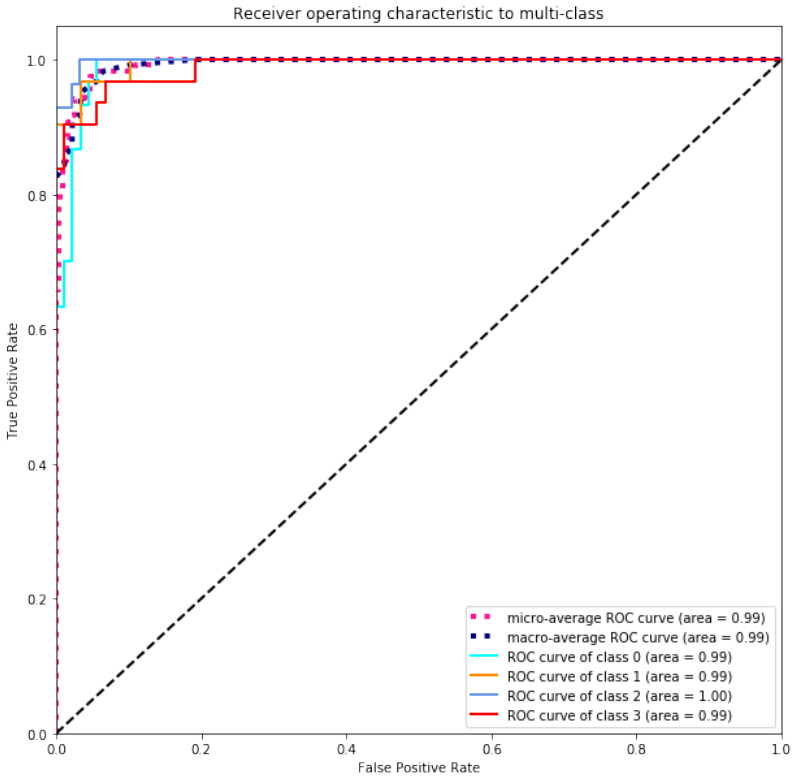
Receiver operating characteristic to multi-class
True Positive Rate
False Positive Rate
0.0
0.2
0.4
0.6
0.8
1.0
micro-average ROC curve (area = 0.99)
macro-average ROC curve (area = 0.99)
ROC curve of class 0 (area = 0.99)
ROC curve of class 1 (area = 0.99)
ROC curve of class 2 (area = 1.00)
ROC curve of class 3 (area = 0.99)

B

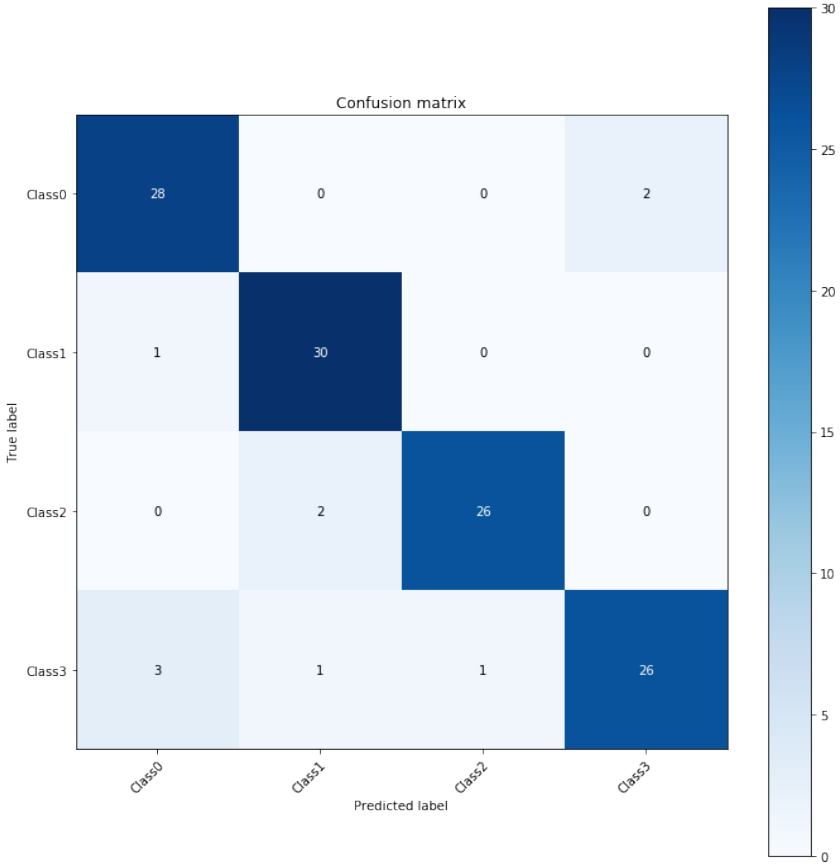
Confusion matrix
Class0
Class1
Class2
Class3
True label
Predicted label
28
0
0
2
1
30
0
0
0
2
26
0
3
1
1
26
30
25
20
15
10
5
0

Figure 10 (A) Receiver operating characteristic plot (B) Confusion matrix for prediction of *E. coli* biofilm inactivation by gas plasma

DNA spectra signature

PAW solution is consisted of nitric, nitrous acid and low level transient RNS like peroxynitrous acid ONOOH, peroxynitrite $ONOO^-$ and ROS (W. F. L. M. Hoeben, 2019). Consistent with this, the bactericidal effect simulated PAW (NOx solution) was significantly lower than PAW, indicating that NO_2, NO_3 species were not the only contributing factors. The DNA spectra profiles of NOx solution and PAW were also compared. Principle Component Analysis was used to reduce the dimensionality of spectra group to allow for data visualization. **Figure 11** showed the PCA result for over 200 spectra scans. In PCA analysis, high dimensional data was projected to a lower dimensional subspace while maximizing the sample variance. P0 to P3 corresponded to DNA spectra for PAW 0, PAW 2, PAW 5 and PAW 10 respectively whereas S0 to S3 corresponded to NOx-0, NOx-2, NOx-5 and NOx-10. DNA spectra in PAW group were all located in the top part of the PC plane plot whereas DNA spectra subjected to simulated PAW treatment were all located in the bottom part of the plot. Within PAW groups, there was a clear cluster separation between different treatment levels. However, for simulated PAW, NOx-2, NOx-5 and NOx-10 were not separated well with PCA analysis. Similar trend has been observed for bacterial inactivation data.

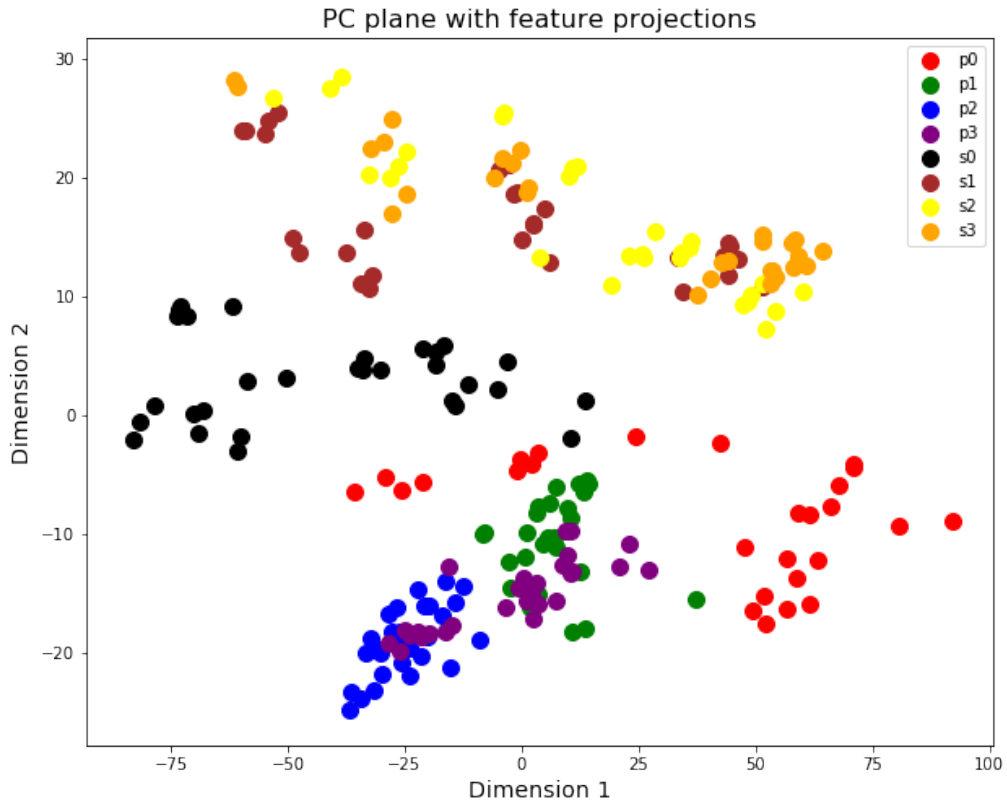

Figure 11 2D visualization of PCA analysis for DNA FTIR spectra with PAW/NOx treatment

Comparing to chemical composition-based prediction

The alternative to predicting bacterial inactivation with NLES would be predicting the inactivation with biochemical measurement of the active species of plasma. In this study, key measurable features related to physiochemical property of PAW including pH, Nitrite, Nitrates concentrations, oxidation-reduction potential (ORP) and Electrical conductivity (EC) were quantified. There is no unique existing parameter that can properly represent PAW activity, but pH, oxidizing-reduction potential and electrical conductivity have shown to provide important insights of PAW activity (Hoeben et al., 2019). Regression model was used to predict bacterial inactivation with these features. With Linear regression 5-fold cross validation, **Figure 12** showed that prediction values for bacterial inactivation overall centered around the measured value, but the predictions were very

far away from the actual values in some cases. Predicting bacterial inactivation through plasma composition is more difficult to implement especially when applying it to large scale industry setting. In comparison, predicting bacterial inactivation via non-living surrogate is easier to implement and has shown to achieve better prediction outcome.

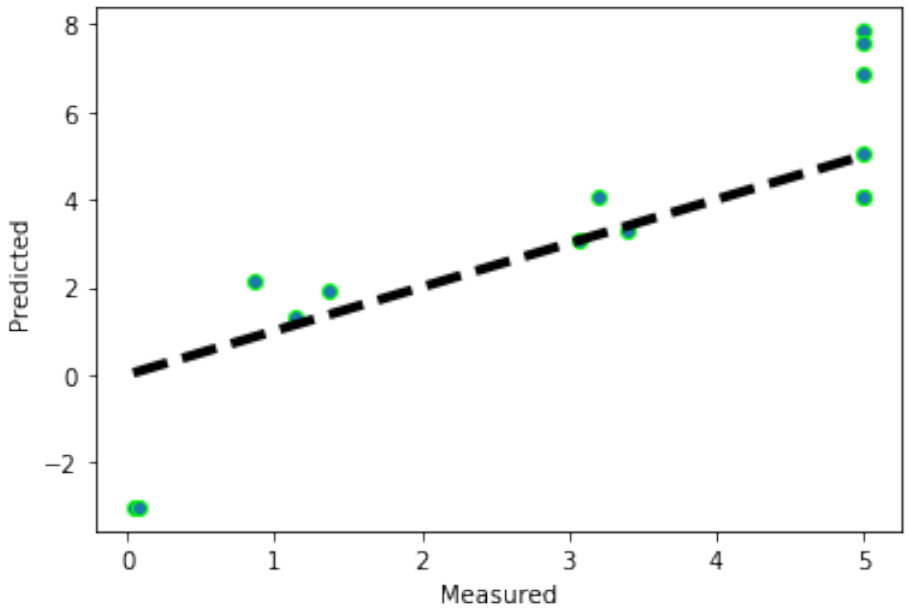

Figure 12 Predicted vs measured E. coli log CFU inactivation using PAW major chemical properties

Conclusion:

In this study, DNA/chitosan layer by layer film was developed as surrogate for validation of bacteria inactivation by plasma treatment both in terms of planktonic cell form as well as biofilm cell form. Plasma treatment studied include direct plasma treatment as well as plasma water treatment. Major findings of this study include: The FTIR spectra of DNA could be used to predict plasma treatment dosage level that DNA was subjected to. Besides, FTIR spectra could also be

used to predict biofilm and planktonic cell inactivation with machine learning algorithm. The machine learning model developed reached around 85%-90% prediction accuracies when tested on unseen data, which indicated good generality of the model regardless of the specific plasma type. Thus, DNA-chitosan film is a promising edible surrogate for validating bacteria and biofilm inactivation. Such surrogate could be embedded in various food contact surface and sampled across many food processing procedures. FTIR data of surrogate could be collected in real time with in-expensive hand-held appliance and thus the surrogate facilities multi-point real time validation of control measure.

References

(Kaatz) Wahlen, L., Parker, A., Walker, D., Pasmore, M., & Sturman, P. (2016). Predictive modeling for hot water inactivation of planktonic and biofilm-associated Sphingomonas parapaucimobilis to support hot water sanitization programs. *Biofouling*. https://doi.org/10.1080/08927014.2016.1192155

An, J. Y., Yong, H. I., Kim, H. J., Park, J. Y., Lee, S. H., Baek, K. H., … Jo, C. (2019). Estimation of inactivation effects against Escherichia coli O157:H7 biofilm by different plasma-treated solutions and post-treatment storage. *Applied Physics Letters*. https://doi.org/10.1063/1.5082657

Bernard, C., Leduc, A., Barbeau, J., Saoudi, B., Yahia, L., & De Crescenzo, G. (2006). Validation of cold plasma treatment for protein inactivation: A surface plasmon resonance-based biosensor study. *Journal of Physics D: Applied Physics*. https://doi.org/10.1088/0022-3727/39/16/S04

Binenbaum, Y., Ben-David, G., Gil, Z., Slutsker, Y. Z., Ryzhkov, M. A., Felsteiner, J., …

Cohen, J. T. (2017). Cold atmospheric plasma, created at the tip of an elongated flexible capillary using low electric current, can slow the progression of Melanoma. *PLoS ONE*. https://doi.org/10.1371/journal.pone.0169457

Breiman, L. (2001). Random forests. *Machine Learning*. https://doi.org/10.1023/A:1010933404324

Bridier, A., Briandet, R., Thomas, V., & Dubois-Brissonnet, F. (2011). Resistance of bacterial biofilms to disinfectants: A review. *Biofouling*. https://doi.org/10.1080/08927014.2011.626899

Buckingham-Meyer, K., Goeres, D. M., & Hamilton, M. A. (2007). Comparative evaluation of biofilm disinfectant efficacy tests. *Journal of Microbiological Methods*. https://doi.org/10.1016/j.mimet.2007.04.010

Chmielewski, R. A. N., & Frank, J. F. (2003). Biofilm formation and control in food processing facilities. *Comprehensive Reviews in Food Science and Food Safety*. https://doi.org/10.1111/j.1541-4337.2003.tb00012.x

Dobrynin, D., Fridman, G., Friedman, G., & Fridman, A. (2009). Mechanisms of direct dielectric barrier discharge plasma inactivation of E. coli. *IEEE International Conference on Plasma Science*, *4*, 4244. https://doi.org/10.1109/PLASMA.2009.5227453

Fraise, A. P., Maillard, J. Y., & Sattar, S. A. (2012). *Russell, Hugo & Ayliffe's: Principles and Practice of Disinfection, Preservation and Sterilization*. *Russell, Hugo & Ayliffe's: Principles and Practice of Disinfection, Preservation and Sterilization*. https://doi.org/10.1002/9781118425831

Gautam, R., Vanga, S., Ariese, F., & Umapathy, S. (2015). Review of multidimensional data processing approaches for Raman and infrared spectroscopy. *EPJ Techniques and Instrumentation*. https://doi.org/10.1140/epjti/s40485-015-0018-6

Govaert, M., Smet, C., Walsh, J. L., & Van Impe, J. F. M. (2019). Dual-Species Model Biofilm Consisting of Listeria monocytogenes and Salmonella Typhimurium: Development and Inactivation With Cold Atmospheric Plasma (CAP). *Frontiers in Microbiology*. https://doi.org/10.3389/fmicb.2019.02524

Guo, L., Xu, R., Gou, L., Liu, Z., Zhao, Y., Liu, D., … Kong, M. G. (2018). Mechanism of virus inactivation by cold atmospheric-pressure plasma and plasmaactivated water. *Applied and Environmental Microbiology*. https://doi.org/10.1128/AEM.00726-18

Hawkins, C. L., & Davies, M. J. (2002). Hypochlorite-induced damage to DNA, RNA, and polynucleotides: Formation of chloramines and nitrogen-centered radicals. *Chemical Research in Toxicology*, *15*(1), 83–92. https://doi.org/10.1021/tx015548d

Hoarau, M., Badieyan, S., & Marsh, E. N. G. (2017). Immobilized enzymes: Understanding enzyme-surface interactions at the molecular level. *Organic and Biomolecular Chemistry*. https://doi.org/10.1039/c7ob01880k

Hoeben, W. F. L. M., van Ooij, P. P., Schram, D. C., Huiskamp, T., Pemen, A. J. M., & Lukeš, P. (2019). On the Possibilities of Straightforward Characterization of Plasma Activated Water. *Plasma Chemistry and Plasma Processing*. https://doi.org/10.1007/s11090-019-09976-7

Jamal, M., Tasneem, U., Hussain, T., & Andleeb, and S. (2015). Bacterial Biofilm: Its Composition, Formation and Role in Human Infections. *Research & Reviews: Journal of*

Microbiology and Biotechnology.

Kamgang-Youbi, G., Herry, J. M., Meylheuc, T., Brisset, J. L., Bellon-Fontaine, M. N., Doubla, A., & Naïtali, M. (2009). Microbial inactivation using plasma-activated water obtained by gliding electric discharges. *Letters in Applied Microbiology*. https://doi.org/10.1111/j.1472-765X.2008.02476.x

Kamgang, J. O., Briandet, R., Herry, J. M., Brisset, J. L., & Naïtali, M. (2007). Destruction of planktonic, adherent and biofilm cells of Staphylococcus epidermidis using a gliding discharge in humid air. *Journal of Applied Microbiology*. https://doi.org/10.1111/j.1365-2672.2007.03286.x

LeChevallier, M. W., Cawthon, C. D., & Lee, R. G. (1988). Inactivation of biofilm bacteria. *Applied and Environmental Microbiology*. https://doi.org/10.1128/aem.54.10.2492-2499.1988

Li, H., & Phung, D. (2014). Journal of Machine Learning Research: Preface. *Journal of Machine Learning Research*, *39*(2014), i–ii.

Liao, L. B., Chen, W. M., & Xiao, X. M. (2007). The generation and inactivation mechanism of oxidation-reduction potential of electrolyzed oxidizing water. *Journal of Food Engineering*. https://doi.org/10.1016/j.jfoodeng.2006.01.004

Lin, C. M., Chu, Y. C., Hsiao, C. P., Wu, J. S., Hsieh, C. W., & Hou, C. Y. (2019). The optimization of plasma-activated water treatments to inactivate Salmonella enteritidis (ATCC 13076) on shell eggs. *Foods*. https://doi.org/10.3390/foods8100520

Lin, Q. K., Ren, K. F., & Ji, J. (2009). Hyaluronic acid and chitosan-DNA complex multilayered

thin film as surface-mediated nonviral gene delivery system. *Colloids and Surfaces B: Biointerfaces*. https://doi.org/10.1016/j.colsurfb.2009.07.036

Lipiec, E., Kowalska, J., Lekki, J., Wiecheć, A., & Kwiatek, W. M. (2012). FTIR microspectroscopy in studies of DNA damage induced by proton microbeam in single PC-3 cells. In *Acta Physica Polonica A*. https://doi.org/10.12693/APhysPolA.121.506

Liu, Y., & Hu, N. (2007). Loading/release behavior of (chitosan/DNA)n layer-by-layer films toward negatively charged anthraquinone and its application in electrochemical detection of natural DNA damage. *Biosensors and Bioelectronics*, *23*(5), 661–667. https://doi.org/10.1016/j.bios.2007.07.009

Lu, H., Patil, S., Keener, K. M., Cullen, P. J., & Bourke, P. (2014). Bacterial inactivation by high-voltage atmospheric cold plasma: Influence of process parameters and effects on cell leakage and DNA. *Journal of Applied Microbiology*. https://doi.org/10.1111/jam.12426

Ma, M., Zhang, Y., Lv, Y., & Sun, F. (2020). The key reactive species in the bactericidal process of plasma activated water. *Journal of Physics D: Applied Physics*. https://doi.org/10.1088/1361-6463/ab703a

Ma, R., Yu, S., Tian, Y., Wang, K., Sun, C., Li, X., … Fang, J. (2016). Effect of Non-Thermal Plasma-Activated Water on Fruit Decay and Quality in Postharvest Chinese Bayberries. *Food and Bioprocess Technology*. https://doi.org/10.1007/s11947-016-1761-7

Mackey, E. D., & Seacord, T. F. (2017). Guidelines for using stainless steel in the water and desalination industries. *Journal - American Water Works Association*, *109*(5), E158–E169. https://doi.org/10.5942/jawwa.2017.109.0044

Mello, M. L. S., & Vidal, B. C. (2012). Changes in the infrared microspectroscopic characteristics of DNA caused by cationic elements, different base richness and single-stranded form. *PLoS ONE*. https://doi.org/10.1371/journal.pone.0043169

Miranda, K. M., Espey, M. G., & Wink, D. A. (2001). A rapid, simple spectrophotometric method for simultaneous detection of nitrate and nitrite. *Nitric Oxide - Biology and Chemistry*. https://doi.org/10.1006/niox.2000.0319

Niemira, B. A., Boyd, G., & Sites, J. (2014). Cold plasma rapid decontamination of food contact surfaces contaminated with salmonella biofilms. *Journal of Food Science*. https://doi.org/10.1111/1750-3841.12379

Nimse, S. B., Song, K., Sonawane, M. D., Sayyed, D. R., & Kim, T. (2014). Immobilization techniques for microarray: Challenges and applications. *Sensors (Switzerland)*, *14*(12), 22208–22229. https://doi.org/10.3390/s141222208

Nocker, A., Shah, M., Dannenmann, B., Schulze-Osthoff, K., Wingender, J., & Probst, A. J. (2018). Assessment of UV-C-induced water disinfection by differential PCR-based quantification of bacterial DNA damage. *Journal of Microbiological Methods*. https://doi.org/10.1016/j.mimet.2018.03.007

Norwood, D. E., & Gilmour, A. (2000). The growth and resistance to sodium hypochlorite of Listeria monocytogenes in a steady-state multispecies biofilm. *Journal of Applied Microbiology*, *88*(3), 512–520. https://doi.org/10.1046/j.1365-2672.2000.00990.x

Oh, J. S., Szili, E. J., Ogawa, K., Short, R. D., Ito, M., Furuta, H., & Hatta, A. (2018). UV-vis spectroscopy study of plasma-activated water: Dependence of the chemical composition on plasma exposure time and treatment distance. *Japanese Journal of Applied Physics*.

https://doi.org/10.7567/JJAP.57.0102B9

Oldenhof, H., Schütze, S., Wolkers, W. F., & Sieme, H. (2016). Fourier transform infrared spectroscopic analysis of sperm chromatin structure and DNA stability. *Andrology*. https://doi.org/10.1111/andr.12166

Paleček, E., Fojta, M., Tomschik, M., & Wang, J. (1998). Electrochemical biosensors for DNA hybridization and DNA damage. In *Biosensors and Bioelectronics*. https://doi.org/10.1016/S0956-5663(98)00017-7

Patel AD, D. A. (2015). Stainless Steel for Dairy and Food Industry: A Review. *Journal of Material Science & Engineering*, *04*(05), 10–13. https://doi.org/10.4172/2169-0022.1000191

Rodríguez, R. A., Bounty, S., & Linden, K. G. (2013). Long-range quantitative PCR for determining inactivation of adenovirus 2 by ultraviolet light. *Journal of Applied Microbiology*. https://doi.org/10.1111/jam.12169

Rosenblum, L. A. (1935). the Surface Inactivation of Catalase. *Journal of Biological Chemistry*, *109*(2), 635–642.

Sassa, A., Kamoshita, N., Matsuda, T., Ishii, Y., Kuraoka, I., Nohmi, T., … Yasui, M. (2013). Miscoding properties of 8-chloro-2′-deoxyguanosine, a hypochlorous acid-induced DNA adduct, catalysed by human DNA polymerases. *Mutagenesis*. https://doi.org/10.1093/mutage/ges056

Shintani, H., Sakudo, A., Burke, P., & McDonnell, G. (2010). Gas plasma sterilization of microorganisms and mechanisms of action. *Experimental and Therapeutic Medicine*.

https://doi.org/10.3892/etm.2010.136

Smet, C., Govaert, M., Kyrylenko, A., Easdani, M., Walsh, J. L., & Van Impe, J. F. (2019). Inactivation of single strains of listeria monocytogenes and salmonella typhimurium planktonic cells biofilms with plasma activated liquids. *Frontiers in Microbiology*. https://doi.org/10.3389/fmicb.2019.01539

Spoering, A. L., & Lewis, K. (2001). Biofilms and planktonic cells of Pseudomonas aeruginosa have similar resistance to killing by antimicrobials. *Journal of Bacteriology*. https://doi.org/10.1128/JB.183.23.6746-6751.2001

Stapelmann, K., Fiebrandt, M., Raguse, M., Awakowicz, P., Reitz, G., & Moeller, R. (2013). Utilization of low-pressure plasma to inactivate bacterial spores on stainless steel screws. *Astrobiology*. https://doi.org/10.1089/ast.2012.0949

Thirumdas, R., Kothakota, A., Annapure, U., Siliveru, K., Blundell, R., Gatt, R., & Valdramidis, V. P. (2018). Plasma activated water (PAW): Chemistry, physico-chemical properties, applications in food and agriculture. *Trends in Food Science and Technology*, *77*(March), 21–31. https://doi.org/10.1016/j.tifs.2018.05.007

Trinetta, V., Vaid, R., Xu, Q., Linton, R., & Morgan, M. (2012). Inactivation of Listeria monocytogenes on ready-to-eat food processing equipment by chlorine dioxide gas. *Food Control*. https://doi.org/10.1016/j.foodcont.2012.02.008

Xiang, Q., Kang, C., Niu, L., Zhao, D., Li, K., & Bai, Y. (2018). Antibacterial activity and a membrane damage mechanism of plasma-activated water against Pseudomonas deceptionensis CM2. *LWT*. https://doi.org/10.1016/j.lwt.2018.05.059

Zhang, Q., Ma, R., Tian, Y., Su, B., Wang, K., Yu, S., … Fang, J. (2016). Sterilization Efficiency of a Novel Electrochemical Disinfectant against Staphylococcus aureus. *Environmental Science and Technology*. https://doi.org/10.1021/acs.est.5b05108

Zhou, R., Zhou, R., Prasad, K., Fang, Z., Speight, R., Bazaka, K., & Ostrikov, K. (2018). Cold atmospheric plasma activated water as a prospective disinfectant: The crucial role of peroxynitrite. *Green Chemistry*. https://doi.org/10.1039/c8gc02800a

Ref:

https://ifst.onlinelibrary.wiley.com/doi/full/10.1111/ijfs.13903

https://onlinelibrary.wiley.com/doi/pdf/10.1002/jsfa.9138

Yong HI, Kim H-J, Park S, Alahakoon AU, Kim K, Choe W et al., Evaluation of pathogen inactivation on sliced cheese induced by encapsulated atmospheric pressure dielectric barrier discharge plasma. Food Microbiol 46:46–50 (2015

Lu: Bacterial inactivation by high - voltage atmospheric cold plasma: influence of process parameters and effects on cell leakage and DNA

Process validation enables the transition of plasma from lab to industry;

Translation of plasma technology from the lab to the food industry

Joshi: Nonthermal dielectric-barrier discharge plasma-induced inactivation involves oxidative DNA damage and membrane lipid peroxidation in Escherichia coli.

Joshi SG, Cooper M, Yost A, Paff M, Ercan UK, Fridman G, Friedman G, Fridman A, Brooks AD

Han: Mechanisms of Inactivation by High-Voltage Atmospheric Cold Plasma Differ for Escherichia coli and Staphylococcus aureus

Thirumdas: Plasma activated water (PAW): Chemistry, physico-chemical properties, applications in food and agriculture